Available online at www.sciencedirect.com
SCIENCE DIRECT
Journal of Catalysis 230 (2005) 384–397
JOURNAL OF CATALYSIS
www.elsevier.com/locate/jcat

Epoxidation of styrene with molecular oxygen catalyzed by cobalt(II)-containing molecular sieves

Qinghu Tang, Qinghong Zhang, Hongli Wu, Ye Wang *

State Key Laboratory of Physical Chemistry of Solid Surfaces and Department of Chemistry, College of Chemistry and Chemical Engineering, Xiamen University, Xiamen 361005, China

Received 11 September 2004; revised 15 December 2004; accepted 16 December 2004

Available online 25 January 2005

Abstract

Co-containing molecular sieves, mainly Co–faujasite zeolite and Co-MCM-41, have been studied for the epoxidation of styrene with molecular oxygen. Characterizations with XRD, TEM, laser-Raman, XPS, and H_2-TPR suggest that the cobalt introduced into MCM-41 by a template-ion exchange method resembles that exchanged in the faujasite zeolite and exists in the single-site Co(II) state, whereas the sample prepared by the impregnation method contains a large proportion of Co_3O_4. The Co(II) sites located in the molecular sieves catalyze the epoxidation of styrene by oxygen with higher activity than Co_3O_4 (ca. 2.6 times based on the same cobalt amount). On the other hand, in homogeneous reactions, $Co(NO_3)_2$ and $Co(Ac)_2$ are almost inactive for the conversion of styrene with oxygen, whereas $CoCl_2$ and $Co(acac)_3$ show some activity, but the selectivity for epoxide is remarkably lower as compared with the Co(II)-containing molecular sieves. Among various oxidants examined, oxygen is found to be the best one for the epoxidation of styrene over the Co(II)-containing molecular sieve catalysts. The solvent plays an important role in epoxidation, and superior catalytic performances have been obtained with an acylamide such as *N*,*N*-dimethylformamide (DMF) as the solvent. The oxygen species with a radical nature generated by the activation of molecular oxygen over the solvent-coordinated Co(II) site has been proposed for the epoxidation reactions.

Keywords: Epoxidation; Styrene; Molecular oxygen; Cobalt(II)-containing molecular sieves; Faujasite zeolites; MCM-41

1. Introduction

The development of effective catalysts for the epoxidation of alkenes to epoxides, which are among the most useful synthetic intermediates, is an important but difficult task in catalysis. Several methods have been developed for the production of epoxides in industry. In the "chlorohydrin" process, epoxides are produced by the intramolecular etherification of chlorohydrins formed by the reaction of alkenes with hypochlorous acid. In the Halcon-Acro and Sumitomo processes, alkyl hydroperoxides are used as oxidants for epoxidation [1]. Although recycling of the co-product (alcohol) has been realized in the Sumitomo process, the need for treatment of large amounts of by-products in these processes has led to the search for other environmentally benign methods, and many intriguing systems have been reported for the epoxidation of alkenes with H_2O_2 [1–7], O_2 combined with a sacrificial reductant, e.g., O_2–H_2 [8–13], O_2–Zn powder [14] or an O_2–organic reductant such as alcohol or aldehyde [15–19], and recently N_2O [20–22] over suitable catalysts. Because of environmental, safety, and economic concerns, however, the utilization of O_2 alone for a catalytic epoxidation is most desirable.

So far, only very few studies have achieved epoxidation by O_2 in the absence of a sacrificial co-reductant. Two ruthenium complexes, Ru(VI)(TMP)$(O)_2$ (where TMP is tetramesitylporphyrin) and *cis*-[Ru(dmp)$_2$(S)$_2$](PF$_6$)$_2$ (where S = H_2O, CH_3CN and dmp is 2,9-dimethyl-1,10-phenanthroline), were reported to catalyze the aerobic epoxidation of alkenes without the need for a co-reductant [23,24]. Recently, ruthenium- and iron-substituted polyoxometalates were

* Corresponding author. Fax: +86 592 2183047.
E-mail address: yewang@jingxian.xmu.edu.cn (Y. Wang).

0021-9517/$ – see front matter
doi:10.1016/j.jcat.2004.12.017

shown to exhibit good catalytic performance in the epoxidation of alkenes by O_2 alone [25,26].

Cobalt ions and complexes are known to catalyze the selective oxidation of alkanes and alkylbenzenes efficiently to organic oxygenates by O_2 [27]. On the other hand, oxidation of alkenes with O_2, catalyzed by cobalt or other transition metals or transition-metal compounds, generally leads to allylic oxidation products in the first step and consequently produces a high degree of oxidized polymers and cleaved products via autooxidation [27,28]. Budnik and Kochi [29] once reported epoxide formation during the oxidation of *tert*-butylethylene, norbornylene, and 1,1-dineopentylethylene, with O_2 catalyzed by Co(III) acetylacetonate (acac), the allylic oxidation of which was difficult to achieve. Reetz and Töllner showed that $Co(acac)_3$ catalyzed the oxidation of styrene only to benzoic acid and benzaldehyde with O_2 at 343 K in THF [30]. Cobalt(II) complexes exhibited high reactivity for the epoxidation of various alkenes by *tert*-butyl hydroperoxide (TBHP) and iodosylbenzene [31,32]. Cobalt salen-type complexes were reported to show catalytic activity for the epoxidation of alkenes by O_2, but a sacrificial reductant was necessary [33].

As for heterogeneous catalysis, many transition metal-based, especially cobalt-based, catalysts have been studied for the selective oxidation of alkanes such as cyclohexane [34–37], but only very few studies contribute to the epoxidation of alkenes by O_2. Raja et al. [38] developed a MAlPO-36 (M = Co or Mn) catalyst effective for the epoxidation of cyclohexene and other alkenes in the presence of an excess of sacrificial aldehyde, based on the work of Yamada et al. [39], who used a homogeneous Ni(II) complex as the catalyst. It is argued that the sacrificial aldehyde is converted to the corresponding peroxy radical, and then the radical induces a specific free radical-based epoxidation [38]. A CoO_x-MCM-41 prepared by ultrasonic deposition–precipitation of cobalt tricarbonyl nitrosyl in decalin was once reported to catalyze the epoxidation of alkenes by O_2 in the presence of an excess of isobutyraldehyde, which functioned as the sacrificial reductant [40]. Recently, Pruss et al. [41] reported that several cobalt complexes immobilized on HMS modified by organic amines could catalyze the epoxidation of alkenes with O_2 and gave moderate selectivity for epoxides in the epoxidation of styrene.

Recently we found and communicated that Co^{2+}-exchanged faujasite zeolites could efficiently catalyze the epoxidation of styrene with O_2 [42]. Our subsequent investigations showed that Co-MCM-41 prepared by a template-ion exchange method was also effective in the same reaction and even exhibited a higher turnover number at lower cobalt content. In the present paper, we report in detail the characterization and the catalysis of these cobalt-containing molecular sieves in the epoxidation of styrene with O_2.

2. Experimental

2.1. Materials

Parent faujasite zeolites, including NaX with a Si/Al ratio of 1.3 and NaY with a Si/Al ratio of 2.8, were prepared via hydrothermal synthesis with $NaSiO_3 \cdot 9H_2O$, $NaAlO_2$, NaOH, and H_2O as starting materials. The molar ratios of Na_2O:Al_2O_3:SiO_2:H_2O in the synthesis mixtures were 4.8:1:3.7:180 and 8:1:10:160 for the syntheses of NaX and NaY, respectively. After hydrothermal synthesis, the NaX or NaY was washed with deionized water, dried at 313 K in vacuum, and calcined at 823 K in air for 6 h. Cobalt or another transition metal ion was introduced into the faujasite zeolite by ion exchange at room temperature in an aqueous solution of metal nitrate for 24 h. The concentration of the aqueous solution was regulated to control the degree of ion exchange and the cobalt or other transition metal content in the sample [43]. After filtration, washing thoroughly with deionized water, and drying at 313 K in vacuum for 24 h, the sample prepared by the ion-exchange method (denoted as Co^{2+}–NaX or Co^{2+}–NaY) was obtained.

Cobalt was introduced into MCM-41 by a template-ion exchange (TIE) method. This method is based on the idea that the cationic surfactants in the as-synthesized S^+I^- type of mesoporous materials typified by MCM-41 can be partially replaced through ion exchange by other inorganic cations. Metal (M) ions such as Mn^{2+} [44–46], VO^{2+} [47–49], Fe^{3+} [50,51], and Cr^{3+} [52] have been introduced into MCM-41 with the TIE method. Since there is no cation-exchanging site in the purely silicious MCM-41 after the calcination to remove the organic surfactant, the introduced hetero-metal component may not exist in the single-site state like a cation in the cation-exchanging site of zeolite. Actually, we found that although the TIE method resulted in highly dispersed vanadyl species [48] or Mn^{2+} [46] on the inner surface of MCM-41, the introduced iron [51] and chromium [52] aggregated to form iron oxide clusters and polychromate species, respectively, after calcination. Therefore, the final state of cobalt introduced by the TIE method requires characterization. In our experiments, MCM-41 was first synthesized by a hydrothermal method by the procedure described previously [48]. Then the as-synthesized (uncalcined) MCM-41 containing ca. 50 wt% template (hexadecyltrimethyl ammonium ion, no Na^+ and Br^- remained) was added to an ethanolic solution of cobalt(II) nitrate or other transition metal nitrate and stirred vigorously at 333 K for 6 h for ion exchanging between the cationic template and the Co^{2+} or other transition metal ions. After the ion exchange, the as-synthesized Co-MCM-41 was separated by filtration, followed by repeated washing with deionized water, and drying in vacuum at 313 K for 24 h. The sample was finally calcined at 823 K in air for 6 h to remove the remaining organic template [48]. It should be noted that no carbon or nitrogen remained in the calcined samples.

For comparison, samples of Co/MCM-41 and Co/Cab-O-Sil were prepared by the conventional wet impregnation method. The powdery MCM-41 or Cab-O-Sil (M5, a nonporous silica purchased from Acros Organics) calcined at 823 K was immersed in an aqueous solution of cobalt(II) nitrate, stirred for 3 h, and allowed to rest for 20 h. The impregnated powder was obtained by heating at 333 K to evaporate water, followed by drying in vacuum at 313 K and calcination at 823 K for 6 h.

2.2. Characterizations

The content of cobalt in each sample was determined by atomic absorption spectroscopic analysis on a WFX-1C spectrometer after the sample was completely dissolved with a small amount of hydrofluoric acid and then diluted nitric acid. The conventional elemental analyses for carbon and nitrogen were performed with a Thermo Quest (Italia) EA1110 analyzer.

Powder X-ray diffraction (XRD) patterns were measured with a Philips X'Pert Pro Super X-ray diffractometer equipped with X'Celerator and Xe detection systems. Cu-K_α radiation (40 kV and 40 mA) was used as the X-ray source.

Properties of porous structures were derived from N_2-sorption measurements at 77 K with a Micromeritics Tristar 3000 surface area and a porosimetry analyzer for mesoporous materials and a Micromeritics ASAP 2010M system for microporous materials. In each case, the sample was outgassed under vacuum at 573 K for 3 h before N_2 adsorption. Pore size distributions for mesoporous materials were evaluated from the desorption isotherms by the BJH method, and those for microporous materials were evaluated by the HK method.

Transmission electron microscopy (TEM) with X-ray energy-dispersive spectroscopic analysis (EDS) was done with a FEI Tecnai 30 electron microscope (Phillips Analytical) operated at an acceleration voltage of 300 kV. Samples for TEM measurements were suspended in ethanol and ultrasonically dispersed. Drops of the suspensions were applied to a copper grid coated with carbon.

X-ray photoelectron spectroscopy (XPS) was measured with a PHI Quantum 2000 Scanning ESCA Microprobe (Physical Electronics) and monochromatic Al-K_α radiation ($h\nu = 1846.6$ eV, 25 W). The background pressure in the analysis chamber was lower than 1×10^{-7} Pa. The X-ray beam diameter was 100 μm, and the pass energy was 29.35 eV for each analysis. The binding energy was calibrated with a C1*s* photoelectron peak at 284.6 eV as a reference.

Raman spectroscopic measurements were carried out with a Renishaw Raman System 1000R. A laser at 514.5 nm was used as the excitation source. A laser output of 30 mW was used, and the maximum incident power at the sample was approximately 6 mW in each measurement.

Temperature-programmed reduction with H_2 (H_2-TPR) was performed with a flow system equipped with a TCD detector. Typically, 100 mg of sample was first pretreated in a quartz reactor with a gas flow containing O_2 and N_2 at 823 K for 1 h followed by purging with pure N_2. After cooling to ca. 300 K, a H_2–Ar (5% H_2) mixture was introduced into the reactor, and the temperature was raised to 1200 K at a rate of 10 K min^{-1}.

Diffuse reflectance UV–visible (DR UV–vis) spectra were recorded with a Varian-Cary 5000 spectrometer equipped with a diffuse reflectance accessory. The spectra were collected in 200–800 nm with $BaSO_4$ as a reference. UV–vis absorption spectroscopic measurements in solution were performed with a Beckman DU-7400 spectrometer, and the spectra were recorded in 200–800 nm.

Fourier transform infrared (FTIR) spectra were recorded with a Nicolet 740SX FTIR instrument with a MCT-B detector. Measurements were carried out at a resolution of 4 cm^{-1} with a total of 32 scans per spectrum.

2.3. Catalytic reactions

The epoxidation of styrene with O_2 was carried out with a round-bottomed glass flask reactor. In a typical run, a measured amount of catalyst was added to the reactor, which was precharged with the desired amount of reactant and solvent, typically *N*,*N*-dimethylformamide (DMF), at the desired temperature. We started the reaction by bubbling O_2 or O_2 diluted with N_2 into the liquid. The reactant mixture was stirred vigorously during the reaction. After the reaction, the catalyst was filtered off, and the liquid organic products were quantified with a gas chromatograph (Shimadzu 14B) equipped with a capillary column (DB-5, 30 M × 0.25 mm × 0.25 μm) and a FID detector, with toluene as an internal standard. In most cases, styrene oxide and benzaldehyde were obtained as the two main products. The turnover number (TON) was calculated from the moles of styrene converted per mole of cobalt contained in the catalyst.

3. Results and discussion

3.1. The content of cobalt introduced and the change in porous structure after cobalt introduction

Table 1 summarizes the content of cobalt introduced in some samples. For the NaX zeolite, if all of the Na^+ ions are replaced with Co^{2+}, a maximum cobalt content of ca. 13.5 wt% can be obtained. When the number of Co^{2+} in the solution used for exchange was overwhelmingly lower than the exchangeable sites, the exchange took place with high efficiency, and almost all of the Co^{2+} ions in the solution could be incorporated into the zeolite. As the degree of exchange became higher, Co^{2+} ions were exchanged into the zeolite with greater difficulty. Thus, only ca. 65% of the degree of exchange could be achieved for the Co^{2+}–NaX in a single exchange process, corresponding to a sample with a

Table 1
Physical properties of Co-containing molecular sieves

Sample[a]	Co content expected (wt%)	Co content in sample (wt%)	Surface area ($m^2\ g^{-1}$)	Pore volume ($cm^3\ g^{-1}$)	Pore diameter (nm)
NaX	–	–	608	0.30	0.81
Co^{2+}–NaX (2.6)	2.7	2.6	625	0.32	0.83
Co^{2+}–NaX (5.7)	5.9	5.7	640	0.33	0.88
Co^{2+}–NaX (8.8)	29.4	8.8	647	0.33	0.90
NaY	–	–	686	0.36	0.87
Co^{2+}–NaY	29.5	6.2	722	0.38	0.90
MCM-41	–	–	1278	0.94	3.1
Co-MCM-41 (0.035)	0.48	0.035	1238	0.89	3.1
Co-MCM-41 (0.26)	0.97	0.26	1162	0.92	3.0
Co-MCM-41 (0.78)	1.92	0.78	1143	0.85	3.0
Co-MCM-41 (2.1)	5.77	2.1	961	0.74	3.0
Co-MCM-41 (5.6)	10.9	5.6	689	0.66	2.9
Co/Cab-O-Sil (5.6)	5.6	5.6	166	–	–
Co/Cab-O-Sil (8.8)	8.8	8.8	152	–	–
Co/MCM-41 (5.6)	5.6	5.6	764	0.61	2.7

[a] The number in the parenthesis after each sample denotes the cobalt content in weight percentage.

cobalt content of 8.8 wt%. Similarly, the maximum degree of exchange for the Co^{2+}–NaY was ca. 71% in a single exchange, corresponding to a sample with cobalt content of 6.2 wt%. Further increases in the amount of Co^{2+} in the solution could not significantly increase the cobalt content in the final samples.

On the other hand, only a very small fraction of cobalt could be incorporated into MCM-41 during the TIE process when a solution with a low concentration of Co^{2+} was used for exchange. For example, less than 10% of Co^{2+} in the solution was incorporated into the final sample during the synthesis of the Co-MCM-41 with a Co content of 0.035 wt%. This fraction became larger with increasing Co^{2+} concentration in the solution. The tendency observed in the TIE process is different from that observed in the ion exchange for the synthesis of Co^{2+}–NaX as described above. Such a difference may stem from the relatively lower rate of the exchange between the Co^{2+} ions in the ethanolic solution and the organic template cations in the uncalcined MCM-41. Thus the rate of the TIE process was probably very low at a low concentration of Co^{2+} and increased with the concentration. On the other hand, in the case of ion exchange between Co^{2+} and Na^+ in the Na–faujasite zeolite, the exchange probably proceeded very quickly and the degree of exchange was mainly limited by the exchangeable sites in the zeolite under our conditions.

The parameters for porous structures of samples obtained from N_2-sorption at 77 K are also listed in Table 1. The surface area, pore volume, and pore diameter were estimated to be, respectively, 608 $m^2\ g^{-1}$, 0.30 $cm^3\ g^{-1}$, and 0.81 nm for the NaX, and all of these parameters became slightly larger after the partial replacement of the Na^+ with the Co^{2+}. A similar tendency was observed when the Co^{2+}–NaY and NaY were compared. This effect could be explained by the fact that two moles of Na^+ in the cages of zeolite are replaced by only one mole of Co^{2+} during the ion exchange.

MCM-41 exhibited a surface area of 1278 $m^2\ g^{-1}$, a pore volume of 0.94 $cm^3\ g^{-1}$, and pore diameter of 3.1 nm. The surface area and pore volume gradually decreased with an increase in cobalt content in the Co-MCM-41 synthesized by the TIE method. A similar tendency was also observed for the Mn-MCM-41 [46] and the Cr-MCM-41 [52] synthesized by the same method, suggesting the incorporation of a hetero-metal component into mesoporous channels. From the TEM observations, it is clear that for the Co-MCM-41

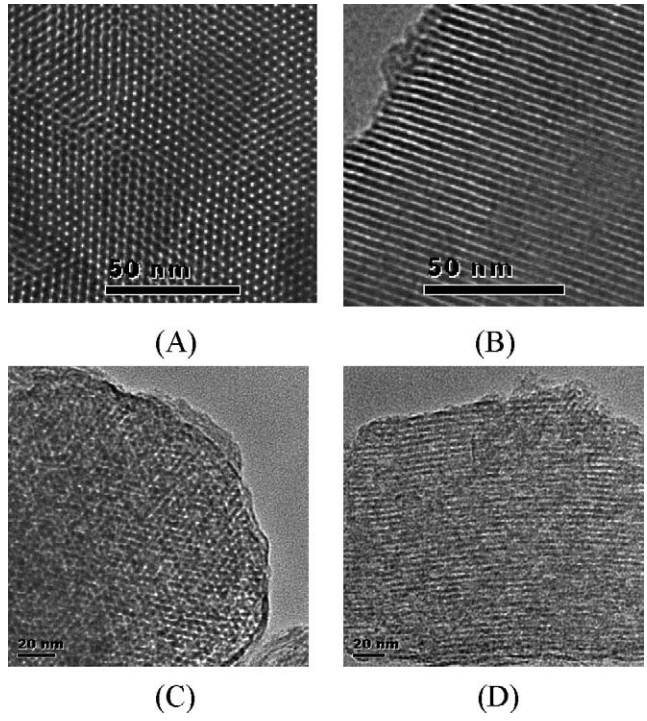

Fig. 1. TEM micrographs of Co-MCM-41 with Co content of 2.1 wt% (A, B) and 5.6 wt% (C, D). (A) and (C) taken with the beam parallel to the pore direction, (B) and (D) taken with the beam perpendicular to the pore direction.

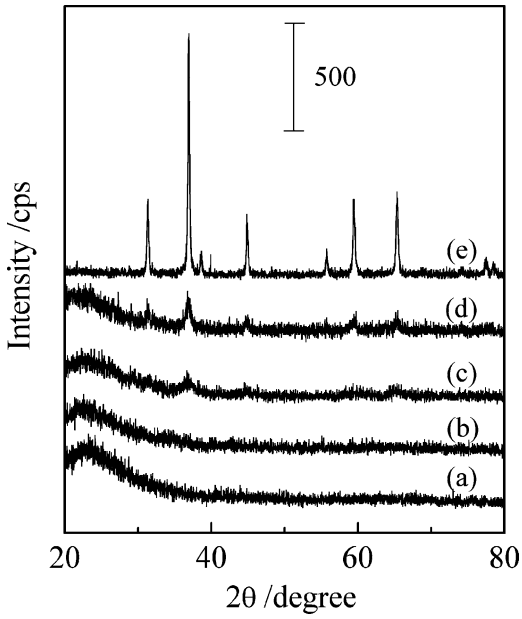

Fig. 2. XRD patterns of Co-containing MCM-41 as well as Co_3O_4, Co/Cab-O-Sil and MCM-41: (a) MCM-41, (b) Co-MCM-41-TIE (Co, 5.6 wt%), (c) Co/MCM-41-IMP (Co, 5.6 wt%), (d) Co/Cab-O-Sil (Co, 5.6 wt%), (e) Co_3O_4.

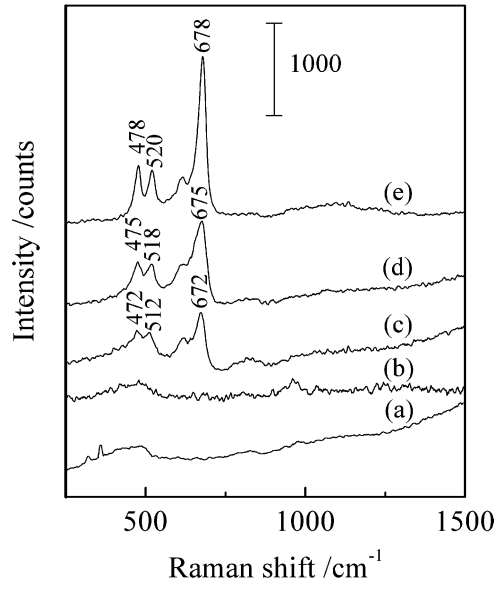

Fig. 3. Raman spectra of Co-containing MCM-41 as well as Co_3O_4, Co/Cab-O-Sil and MCM-41: (a) MCM-41, (b) Co-MCM-41-TIE (Co, 5.6 wt%), (c) Co/MCM-41-IMP (Co, 5.6 wt%), (d) Co/Cab-O-Sil (Co, 5.6 wt%), (e) Co_3O_4.

sample with a Co content of 2.1 wt% (Figs. 1A and B) or less, the hexagonal array of mesoporous channels of MCM-41 is well sustained. However, the loss of order over the long range became obvious for the sample with a Co content of 5.6 wt% (Figs. 1C and D). It should be noted here that the ordered mesoporous structure of MCM-41 could be sustained after the introduction of cobalt by the impregnation method, even with a content of 5.6 wt%.

3.2. Coordination environment and oxidation state of cobalt

XRD investigations for the Co^{2+}–NaX and the Co^{2+}–NaY prepared by ion exchange revealed that only diffraction peaks ascribed to NaX and NaY were observed. This result is consistent with the fact that cobalt ions exchanged into the zeolites are highly dispersed.

Fig. 2 shows XRD patterns for the Co-MCM-41 prepared by the TIE method, along with those for Co/MCM-41, Co/Cab-O-Sil, and Co_3O_4. Only a broad peak due to the amorphous feature of the framework of MCM-41 appeared, and no peak of the crystalline Co_3O_4 was observed for Co-MCM-41-TIE (Co, 5.6 wt%). On the other hand, for the Co/MCM-41 and Co/Cab-O-Sil with the same cobalt content prepared by the impregnation (IMP) method, peaks at ca. 37°, 45°, and 65°, ascribed to the crystalline Co_3O_4, could be discerned. These results indicate that the cobalt species introduced by the TIE method are highly dispersed in MCM-41, whereas aggregated Co_3O_4 particles are formed when cobalt is introduced by the impregnation method.

This is consistent with the TEM observations, which show no large particles located outside the mesopores for the Co-MCM-41-TIE sample, even with a cobalt content of 5.6 wt%, and the EDS measurements reveal homogeneous distributions of cobalt in this sample. However, unlike the Co-MCM-41-TIE sample, although the Co/MCM-41 (Co, 5.6 wt%) prepared by the impregnation could sustain the hexagonal mesoporous structure better, large cobalt oxide particles with size of ca. 10 nm were observed outside the mesoporous channels.

Further insight into the state of cobalt introduced into MCM-41 has been gained from Raman spectroscopic measurements. Fig. 3 shows the Raman spectra of several Co-containing samples. Raman measurements for Co^{2+}–NaX (Co, 8.8 wt%) and the Co^{2+}–NaY (Co, 6.2 wt%) were also attempted, but no useful information could be obtained because of the serious fluorescence, which was possibly due to the high content of aluminum [53]. The crystalline Co_3O_4 exhibited four Raman bands at 478, 520, 601, and 678 cm^{-1}, arising from the vibrations of Co–O bonds [54]. Similar patterns were observed for Co/Cab-O-Sil (Co, 5.6 wt%) and Co/MCM-41 (Co, 5.6 wt%), but the peaks became broader compared with Co_3O_4. Moreover, these Raman bands shifted to lower-wavenumber positions. The broadening and the red-shift of the Raman bands indicate that the size of cobalt oxide particles decreases in the order of Co_3O_4 > Co_3O_4 on the Co/Cab-O-Sil > Co_3O_4 on the Co/MCM-41. The Raman bands of the Co–O vibrations due to cobalt oxide did not appear for the Co-MCM-41-TIE (Co, 5.6 wt%), further supporting the assumption that the cobalt species were highly dispersed in this sample.

The oxidation state of cobalt has been investigated by XPS. Fig. 4 shows the Co 2*p* XPS spectra for several typical Co-containing samples. The binding energy of Co $2p_{3/2}$ for the Co^{2+}–NaX (Co, 8.8 wt%) was 781.7 eV, and the

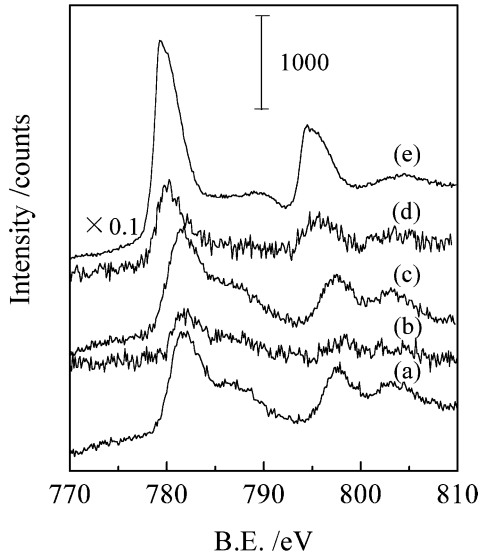

Fig. 4. Co 2*p* XPS spectra of Co-containing molecular sieves as well as Co_3O_4: (a) Co^{2+}–NaX (Co, 8.8 wt%), (b) Co-MCM-41-TIE (Co, 0.78 wt%), (c) Co-MCM-41-TIE (Co, 5.6 wt%), (d) Co/MCM-41-IMP (Co, 5.6 wt%), (e) Co_3O_4.

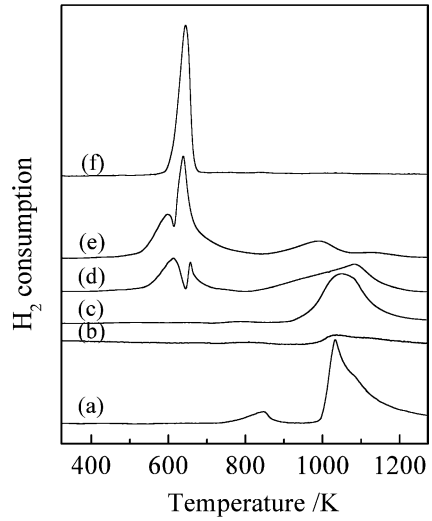

Fig. 5. TPR profiles of Co-containing molecular sieves as well as Co_3O_4 and Co/Cab-O-Sil: (a) Co^{2+}–NaX (Co, 8.8 wt%), (b) Co-MCM-41-TIE (Co, 0.78 wt%), (c) Co-MCM-41-TIE (Co, 5.6 wt%), (d) Co/MCM-41-IMP (Co, 5.6 wt%), (e) Co/Cab-O-Sil (Co, 5.6 wt%), (f) Co_3O_4.

cobalt species with such a binding energy could be assigned to Co(II) in an isolated state, undergoing interactions with the anionic framework of zeolite [55]. It is interesting to note that the Co-MCM-41-TIE samples possess almost the same binding energy of Co 2*p* with the Co^{2+}–NaX sample, suggesting that the cobalt species introduced into MCM-41 by the TIE method are also mainly in the single-site Co(II) state. On the other hand, the Co/MCM-41 prepared by the impregnation method exhibited a binding energy of Co $2p_{3/2}$ close to that for Co_3O_4. This coincides with the conclusion of XRD, TEM, and Raman studies.

The state of cobalt species in the samples prepared by different methods has also been investigated by H_2-TPR. It is known that the reduction of Co^{2+} ions exchanged in zeolites such as NaY [56,57] and Na-ZSM-5 [58] is difficult, and temperatures higher than 800 K are needed in most cases because of the strong interaction between the Co^{2+} and the anionic zeolite framework, whereas the reduction of Co_3O_4 or supported cobalt oxide particles generally occurs at 593–673 K [59–61]. H_2-TPR profiles in Fig. 5 show that, like Co^{2+}–NaX, the Co-MCM-41-TIE samples exhibit a reduction peak at a high temperature (1043 K). This result further suggests that the cobalt species in the Co-MCM-41-TIE are similar to those in the Co^{2+}–NaX and are probably in the single-site Co(II) state.

On the other hand, two reduction peaks at low temperatures (i.e., at 573–673 K) were mainly observed for the Co/Cab-O-Sil and the Co/MCM-41, although Co_3O_4 alone showed only one asymmetrical peak. These two peaks probably stem from the stepwise reduction of the supported Co_3O_4 to CoO and then CoO to Co [60,61]. Two broad reduction peaks could also be discerned at ca. 980 and 1080 K in addition to the peaks at 573–673 K in the H_2-TPR profile for Co/MCM-41 (Co, 5.6 wt%) prepared by impregnation. We tentatively ascribe these high-temperature reduction peaks to the reduction of a small part of isolated Co(II) or some small CoO_x clusters with relatively stronger interaction with the framework of MCM-41. A remarkably weaker peak in the high-temperature region was observed (at ca. 990 K) for Co/Cab-O-Sil (Co, 5.6 wt%). Thus we can speculate that, as compared with Co/Cab-O-Sil, over which most of the cobalt species are in the aggregated Co_3O_4 state, there are more highly dispersed cobalt species over Co/MCM-41.

3.3. Epoxidation of styrene catalyzed by Co^{2+}-exchanged zeolites

Table 2 summarizes the catalytic performances of a variety of catalysts in the epoxidation of styrene with O_2. The comparison among different transition-metal ion-exchanged NaX zeolites (entries 2–7) reveals that Co^{2+}–NaX provides the highest styrene conversion and styrene oxide selectivity. Thus cobalt is a very unique component for the epoxidation of styrene with O_2.

It is known that cobalt salts such as $Co(Ac)_2$ in the liquid phase can catalyze the selective oxidation of alkanes such as cyclohexane with O_2 [27]. We have thus carried out the epoxidation of styrene with the use of homogeneous Co(II) or Co(III) salts by dissolving $Co(Ac)_2$, $Co(NO_3)_2$, $CoCl_2$, and $Co(acac)_3$ (acac = acetylacetone) in the solvent (DMF). It is of interest to note that $Co(Ac)_2$ and $Co(NO_3)_2$ are almost inactive for the conversion of styrene with O_2, whereas $CoCl_2$ and $Co(acac)_3$ show some activity (entries 8–11). Both the styrene conversion and styrene oxide selectivity of $CoCl_2$ and $Co(acac)_3$ were, however, remarkably lower than those of Co^{2+}–NaX. The Co/Cab-O-Sil containing Co_3O_4 as the main cobalt species and Co_3O_4 itself also catalyzed the epoxidation of styrene by O_2 with good selectivity, but styrene conversion was remarkably lower over

Table 2
Epoxidation of styrene with O_2 catalyzed by a variety of catalysts based on zeolites or cobalt[a]

Entry	Catalyst[b]	Styrene conversion (%)	Epoxide selectivity (%)	Turnover number
1	NaX	0.3	42	–
2	Cr^{3+}–NaX (7.7)	18	52	6.0
3	Mn^{2+}–NaX (8.2)	6.1	47	2.0
4	Co^{2+}–NaX (8.8)	44	60	15
5	Ni^{2+}–NaX (8.9)	4.5	49	1.5
6	Cu^{2+}–NaX (10.4)	2.6	42	0.8
7	Zn^{2+}–NaX (9.5)	5.9	47	2.0
8	$Co(Ac)_2$	0.4	0	0.1
9	$Co(NO_3)_2$	0.9	0	0.3
10	$CoCl_2$	15	28	5.1
11	$Co(acac)_3$	10	22	3.4
11	Co_3O_4	17	66	5.5
12	Co/Cab-O-Sil (8.8)	17	60	5.7
13	Co^{2+}–NaY (6.2)	45	62	15
14	Co^{2+}–NaL (4.3)	18	54	6.1
15	Co^{2+}–mordenite (2.9)	16	52	5.4
16	Co^{2+}–beta (1.4)	26	48	8.7

[a] Reaction conditions: the amount of transition metal ions in catalysts was fixed at 0.299 mmol; the amount of NaX, 0.2 g; reaction temperature, 373 K; styrene, 10 mmol; DMF, 20 ml; flow rate of O_2, 3.0 $cm^3\,min^{-1}$; reaction time, 4 h.

[b] The number in the parenthesis after each sample denotes the cobalt content in weight percentage.

these samples. Moreover, we could not raise styrene conversion significantly by increasing the amount of catalyst in the cases of Co/Cab-O-Sil and Co_3O_4.

The comparison among several different Co^{2+}-exchanged zeolites reveals that Co^{2+} ions in the faujasite zeolites (NaX and NaY) exhibit the best catalytic performances in the epoxidation of styrene with O_2. The activity, expressed by the turnover number (TON), decreased in the following sequence: Co^{2+}–NaX ≈ Co^{2+}–NaY > Co^{2+}–beta > Co^{2+}–L ≈ Co^{2+}–mordenite. All of these zeolites possess 12-ring pore windows with apertures of ca. 0.7–0.8 nm, but they have different porous structures. The faujasite and beta zeolites have three-dimensional porous structures, and large voids are formed at the intersections of porous channels in both cases. As compared with the beta zeolite, much larger voids with a diameter of ca. 1.3 nm (known as "supercages") exist in the faujasite zeolites. On the other hand, the L-type zeolite has only one-dimensional pore channels. Although there is an 8-ring channel in the b axis in addition to the main 12-ring channel in the c axis, the pore of mordenite is generally viewed as one-dimensional, since the 8-ring channel in the b axis is highly distorted (0.57 × 0.26 nm). The differences in catalytic performances for Co^{2+} ions exchanged into these zeolites may stem from the different porous structures. It seems likely that the zeolites with larger spaces to accommodate Co(II) sites for reaction (larger reaction spaces) exhibit better catalytic performance.

It is known that the cations in faujasite zeolites can occupy several different types of sites with different locations and potential energies, such as sites I, I′, II, II′, III, and III′

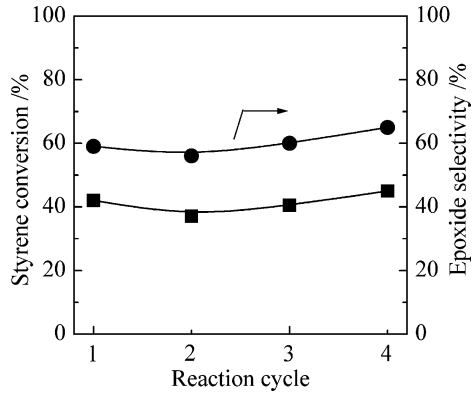

Fig. 6. Repeating uses of Co^{2+}–NaX (Co, 8.8 wt%) for the epoxidation of styrene with O_2: (■) styrene conversion, (●) epoxide selectivity. Reaction conditions: catalyst, 0.2 g; temperature, 373 K; styrene, 10 mmol; DMF, 20 ml; flow rate of O_2, 3.0 ml min^{-1}; reaction time, 4 h.

[62,63]. Sites III, III′, and II are located in the supercages, and the other sites are in the small sodalite cages and the hexagonal prisms of the faujasite. It has been reported that some Co^{2+} ions may migrate from the supercages to the small sodalite cages and the hexagonal prisms with increasing temperature [64,65]. Therefore, the temperature used for the treatment of Co^{2+}–faujasite may affect catalytic performance by changing the distribution of Co^{2+} ions. Our studies on the effect of the treatment temperature [42] further suggest that the Co^{2+} ions located in the spaces with larger sizes (the supercages of faujasite zeolites) exhibit better catalytic performance in the epoxidation reactions.

Repeated runs of the recovered Co^{2+}–NaX for the epoxidation of styrene have been carried out; the results are shown in Fig. 6. Neither styrene conversion nor epoxide selectivity changed significantly in the repeated runs. After the reaction the liquid filtrate was subjected to atomic absorption spectroscopic analysis, and no cobalt could be detected. When the liquid filtrate was used in the reaction instead of the solid catalyst, no significant conversion of styrene was observed. Moreover, Co^{2+} or Co^{3+} ions or compounds added as $Co(Ac)_2$, $Co(NO_3)_2$, $CoCl_2$, or $Co(acac)_3$ are poor homogeneous epoxidation catalysts, as shown in Table 2. We thus speculate that the epoxidation proceeds heterogeneously over the Co^{2+}–faujasite zeolite. On the other hand, the leaching of active component (redox center) from molecular sieve-based catalysts seems to be a serious problem when H_2O_2 or organic hydroperoxide is used as the oxidant for epoxidation, probably because H_2O_2 or organic hydroperoxide has a marked ability to dissolve the redox component, such as vanadium or chromium, from molecular sieves into the liquid phase [66]. Therefore, the use of O_2 as the oxidant in our system also has advantages that increase the stability against leaching for the molecular sieve-based heterogeneous catalysts and may thus provide another opportunity to exploit the redox molecular sieves for liquid-phase-selective oxidation reactions.

Table 3
Epoxidation of styrene with O_2 catalyzed by a variety of catalysts based on MCM-41[a]

Entry	Catalyst[b]	Styrene conversion (%)	Epoxide selectivity (%)	Turnover number
1	MCM-41	4.0	45	–
2	Cr-MCM-41 (1.40)	10	45	19
3	Mn-MCM-41 (0.71)	2.0	31	1.9
4	Fe-MCM-41 (1.06)	16	51	42
5	Co-MCM-41 (0.78)	45	62	169
6	Ni-MCM-41 (2.30)	4.3	40	5.5
7	Cu-MCM-41 (2.20)	0	0	0
8	Zn-MCM-41 (1.91)	5.2	54	8.9

[a] Reaction conditions: the amount of transition metal in catalysts, 0.299 mmol; reaction temperature, 373 K; styrene, 10 mmol; DMF, 20 ml; flow rate of O_2, 3.0 $cm^3\ min^{-1}$; reaction time, 4 h.
[b] The number in the parenthesis after each sample denotes the content of transition metal in weight percentage.

3.4. Epoxidation of styrene catalyzed by Co-MCM-41

Table 3 lists the performances of a variety of catalysts based on MCM-41 in the epoxidation of styrene with O_2. Among various transition metal-containing MCM-41 prepared by the TIE method, Co-MCM-41 was the best for the epoxidation of styrene. The highest styrene conversion and styrene oxide selectivity were obtained over this catalyst. In addition to styrene, benzaldehyde was mainly formed as the by-product.

Table 4 shows the effect of cobalt content on catalytic performances of Co^{2+}–NaX and Co-MCM-41. For the Co^{2+}–NaX catalysts, styrene conversion increased remarkably with cobalt content in the whole range of 0–8.8 wt%. The TON decreased only slightly with cobalt content in these samples. For the Co-MCM-41 series, the increase in cobalt content from 0 to 0.78 wt% also increased styrene conversion and styrene oxide selectivity, but further increases in Co content did not significantly change the catalytic performances. The TON was much higher for the Co-MCM-41 with a lower cobalt content, and it decreased very sharply with cobalt content. This tendency is different from that for the Co^{2+}–NaX series. This difference may arise from different locations of the Co(II) sites in the Co^{2+}–NaX and the Co-MCM-41. As described above, Co(II) in the Co^{2+}–NaX may be located in supercages, sodalite cages, and hexagonal prisms, and only those in supercages may account for the epoxidation of styrene by O_2. On the other hand, the Co(II) sites in Co-MCM-41 are located solely in the mesoporous channels, and all of these can be accessed by the reactants. Thus, as compared with the Co-MCM-41, a larger content of cobalt is needed to obtain the same activity for Co^{2+}–NaX, resulting in a lower TON. The reason for the sharp drop in the TON with an increase in cobalt content in the case of Co-MCM-41 is still not clear at this moment.

As shown in Table 4, the catalytic activity for the epoxidation of styrene by O_2 decreased in the sequence Co-MCM-41 > Co/MCM-41 > Co/Cab-O-Sil with the same cobalt content of 5.6 wt%. As indicated by XRD, TEM, Raman, XPS, and H_2-TPR results described above, cobalt in Co-MCM-41 mainly existed in the single-site Co(II) state, whereas that in Co/Cab-O-Sil mainly aggregated into Co_3O_4 particles. Co/MCM-41 contained Co_3O_4 particles and some highly dispersed cobalt species. Therefore, it is likely that a higher dispersion of cobalt species results in higher catalytic activity. The single-site Co(II) site is the most active site for the epoxidation of styrene by O_2.

Table 4
Effect of cobalt content on catalytic performances for the Co^{2+}–NaX and Co-MCM-41[a]

Entry	Catalyst[b]	Styrene conversion (%)	Epoxide selectivity (%)	Turnover number
1	NaX	0.3	42	–
2	Co^{2+}–NaX (2.6)	21	59	19
3	Co^{2+}–NaX (5.7)	30	64	13
4	Co^{2+}–NaX (8.8)	44	60	15
5	MCM-41	4.0	45	–
6	Co-MCM-41 (0.035)	14	56	1145
7	Co-MCM-41 (0.26)	35	59	401
8	Co-MCM-41 (0.78)	45	62	169
9	Co-MCM-41 (2.1)	43	57	60
10	Co-MCM-41 (5.6)	43	59	23
11	Co/MCM-41 (5.6)	32	58	17
12	Co/Cab-O-Sil (5.6)	16	58	8.5

[a] Reaction conditions: catalysts, 0.2 g; reaction temperature, 373 K; styrene, 10 mmol; DMF, 20 ml; flow rate of O_2, 3.0 $cm^3\ min^{-1}$; reaction time, 4 h.
[b] The number in the parenthesis after each sample denotes the cobalt content in weight percentage.

3.5. Kinetic investigations of the epoxidation of styrene catalyzed by Co^{2+}–NaX

It has been found that Co-MCM-41 shows kinetic behaviors similar to those of the Co^{2+}–NaX catalyst in the epoxidation of styrene with O_2. Here we describe the kinetic results obtained for the Co^{2+}–NaX catalyst with a cobalt content of 8.8 wt%.

Fig. 7 shows the time course for the epoxidation of styrene with O_2 catalyzed by the Co^{2+}–NaX. To measure O_2 consumption during the reaction, N_2 was added to the gas flow and used as an internal standard. The concentrations of O_2 in the gas flow before and during the reaction were determined by gas chromatography. We have observed some uptake of O_2 by the solvent (DMF) in the presence of the Co^{2+}–NaX catalyst without the substrate, and such O_2 uptake would finish in ca. 30 min, suggesting the adsorption of O_2 in our system. In the presence of styrene, both O_2 consumption and styrene conversion increased monotonically. The oxygen balance was determined to be ca. 90%. The selectivities for styrene oxide and benzaldehyde remained almost unchanged with the reaction time, indicating that benzaldehyde might mainly be formed in parallel with styrene oxide.

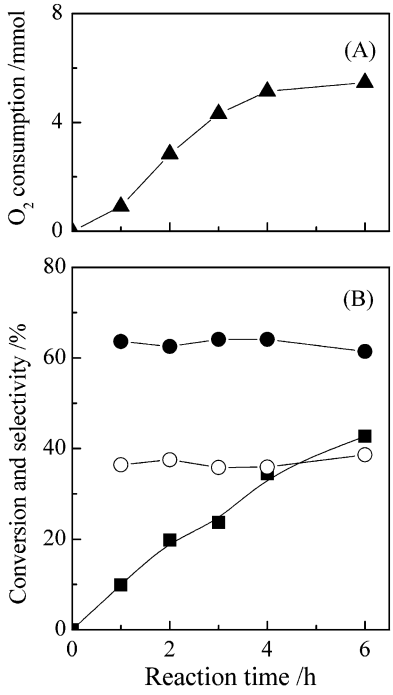

Fig. 7. Time course for (A) O_2 consumption and (B) catalytic performances during the epoxidation of styrene with O_2 catalyzed by the Co^{2+}–NaX (Co, 8.8 wt%): (■) styrene conversion, (●) epoxide selectivity, (○) benzaldehyde selectivity. Reaction conditions: catalyst, 0.2 g; temperature, 373 K; styrene, 15 mmol; DMF, 20 ml; total flow rate of O_2 and N_2, 6.0 ml min^{-1}; ratio of O_2/N_2, 0.85.

The effect of O_2 pressure on the catalytic performances of the Co^{2+}–NaX is shown in Fig. 8. The conversion of styrene increased almost proportionally to O_2 pressure, which was regulated by dilution of O_2 with N_2 at different O_2/N_2 ratios. This confirms that the active oxygen species responsible for epoxidation are generated from the activation of O_2. With the increase in O_2 pressure, the selectivity for styrene oxide decreased slightly, and that for benzaldehyde increased slightly.

Fig. 9 shows the effect of reaction temperature on the catalytic performances of the Co^{2+}–NaX. At temperatures lower than 363 K, not only styrene conversion but also styrene oxide selectivity increased remarkably with the reaction temperature (Fig. 9A). Such increases were decelerated at temperatures higher than 363 K. When the logarithm of styrene conversion rate was plotted against the reciprocal of the reaction temperature, two straight lines with different slopes were required to fit the data (Fig. 9B). The apparent activation energy calculated was 96 kJ mol^{-1} at < 363 K, whereas it decreased to 18 kJ mol^{-1} at > 363 K. Such a low activation energy indicates that the reactions above 363 K are probably rate-determined by the diffusion of reactants to the active sites. We think that this may explain the result that the Co(II) site located in a larger space shows a better catalytic performance.

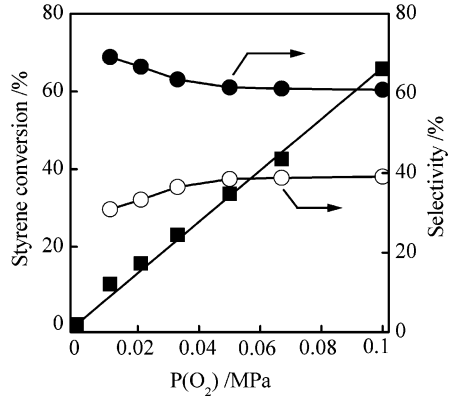

Fig. 8. Effect of O_2 pressure on catalytic performances of the Co^{2+}–NaX (Co, 8.8 wt%) for the epoxidation of styrene with O_2: (■) styrene conversion, (●) epoxide selectivity, (○) benzaldehyde selectivity. Reaction conditions: catalyst, 0.2 g; temperature, 373 K; styrene, 10 mmol; DMF, 20 ml; total flow rate of O_2 and N_2, 6.0 ml min^{-1}; reaction time, 4 h.

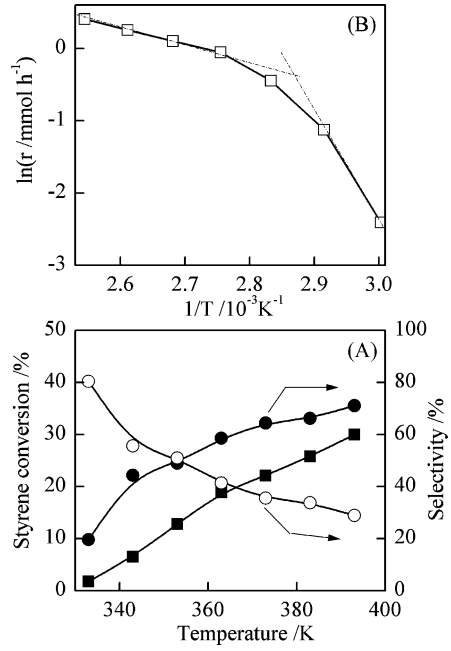

Fig. 9. (A) Effect of temperature on catalytic performances and (B) logarithm of styrene conversion rate versus reciprocal of temperature over the Co^{2+}–NaX (Co, 8.8 wt%): (■) styrene conversion, (●) epoxide selectivity, (○) benzaldehyde selectivity. Reaction conditions: catalyst, 0.2 g; styrene, 10 mmol; DMF, 20 ml; flow rate of O_2, 3.0 ml min^{-1}; reaction time, 2 h.

3.6. Effects of oxidants and solvents on the epoxidation of styrene catalyzed by Co^{2+}–NaX and Co-MCM-41

Table 5 shows the catalytic performances for the epoxidation of styrene with different oxidants over the Co^{2+}–NaX (Co, 8.8 wt%) and the Co-MCM-41 (Co, 0.78 wt%) catalysts. The two catalysts showed very similar features in the epoxidation with different oxidants. No styrene conversion was observed when the reaction was carried out under Ar or a pure N_2 atmosphere without any oxidants (entries 1 and 6). In the case of O_2 over both catalysts (entries 2 and 7),

Table 5
Epoxidation of styrene with various oxidants over the Co^{2+}–NaX (Co, 8.8 wt%) and the Co-MCM-41 (Co, 0.78 wt%)[a]

Entry	Catalyst	Oxidants	Styrene conversion (%)	Epoxide selectivity (%)
1[b]	Co^{2+}–NaX	None	0	–
2	Co^{2+}–NaX	O_2	44	60
3	Co^{2+}–NaX	H_2O_2	21	56
4	Co^{2+}–NaX	TBHP	74	12
5	Co^{2+}–NaX	NaClO	2.6	27
6[b]	Co-MCM-41	None	0	–
7	Co-MCM-41	O_2	45	62
8	Co-MCM-41	H_2O_2	19	66
9	Co-MCM-41	TBHP	79	6.9
10	Co-MCM-41	NaClO	2.1	50

[a] Reaction conditions: catalyst, 0.2 g; reaction temperature, 373 K; styrene, 10 mmol; DMF, 20 ml; flow rate of O_2, 3.0 ml min^{-1}. For other oxidants than O_2, adding 10 mmol instead of bubbling O_2; reaction time, 4 h.
[b] The reaction was carried out under Ar atmosphere without adding an oxidant.

styrene oxide and benzaldehyde were produced. Very low activity was obtained with NaClO over both catalysts (entries 5 and 10). Although styrene conversion was high with TBHP, styrene oxide selectivity was very low over both catalysts (entries 4 and 9). In addition to benzaldehyde (31% and 22% of selectivity over the Co^{2+}–NaX and the Co-MCM-41, respectively), polymeric products were probably among the by-products in the case of TBHP, indicating the occurrence of uncontrollable free radical reactions. H_2O_2 gave reasonably good performance for the epoxidation of styrene (entries 3 and 8), but styrene conversion was lower compared with that observed with O_2 over both catalysts. The rapid decomposition of H_2O_2 into O_2 over the catalysts at the initial stage would be the main reason for the lower activity. Therefore, the current Co-based catalysts are very specific in the activation of O_2 for the epoxidation of alkenes.

Various solvents with relatively low volatility (b.p. > 373 K) have been tested for the epoxidation of styrene by O_2 over the Co^{2+}–NaX (Co, 8.8 wt%) and the Co-MCM-41 (Co, 0.78 wt%) catalysts; the results are summarized in Table 6. The two catalysts exhibited similar catalytic behaviors with different solvents. As shown in Table 6, the solvent played a crucial role in the epoxidation reactions. It is of significance to note that the acylamides, including dimethylformamide (DMF) and dimethylacetamide (DMA), are particularly efficient in providing both high styrene conversion and high epoxide selectivity. Although high styrene conversion could be obtained when dimethyl sulfoxide (DMSO), acetylacetone, and cyclohexanone were used, the selectivity for styrene oxide was low. No reaction occurred when nitrogen- or chloro-containing solvents such as pyridine and monochlorobenzene were used. It should be noted that *tert*-butyl alcohol, a potential co-reductant for the activation of O_2 [67], did not work here. The uniqueness of DMF (or DMA) as the solvent may suggest several possible roles, such as coordination with cobalt sites to form the true active sites during the reaction and/or acting as a co-reductant.

3.7. Coordination of DMF with cobalt(II) sites

There are a few studies on the coordination of DMF or DMA to cobalt(II) complexes [68–70], and such a coordination may affect the ability of O_2 to bind to the cobalt complexes and their redox potential [71,72]. As described above, in our study we found that the solvent played a key role in our search for high catalytic performance in the epoxidation of styrene by O_2 over the Co(II)-containing molecular sieve catalysts. We have thus investigated the possible coordination of DMF to the Co(II) sites located in the NaX zeolite.

Table 6
Epoxidation of styrene by O_2 in different solvents over the Co^{2+}–NaX (Co, 8.8 wt%) and the Co-MCM-41 (Co, 0.78 wt%)[a]

Entry	Catalyst	Solvent	Styrene conversion (%)	Epoxide selectivity (%)
1	Co^{2+}–NaX	*N*,*N*-Dimethylformamide (DMF)	44	60
2	Co^{2+}–NaX	*N*,*N*-Dimethylacetamide (DMA)	45	74
3	Co^{2+}–NaX	Dimethyl sulfoxide (DMSO)	32	1.9
4	Co^{2+}–NaX	Acetylacetone	69	30
5	Co^{2+}–NaX	Cyclohexanone	43	34
6	Co^{2+}–NaX	Pyridine	0	–
7	Co^{2+}–NaX	[1-*n*-Butyl-3-methylimidazolium]PF_6	8	21
8	Co^{2+}–NaX	*tert*-Butyl alcohol	0	–
9	Co^{2+}–NaX	Monochlorbenzene	1.0	48
10	Co-MCM-41	*N*,*N*-Dimethylformamide (DMF)	45	62
11	Co-MCM-41	*N*,*N*-Dimethylacetamide (DMA)	48	67
12	Co-MCM-41	Dimethyl sulfoxide (DMSO)	39	4.7
13	Co-MCM-41	Acetylacetone	46	12
14	Co-MCM-41	Cyclohexanone	29	49
15	Co-MCM-41	Pyridine	0	–
16	Co-MCM-41	[1-*n*-Butyl-3-methylimidazolium]PF_6	13	19
17	Co-MCM-41	*tert*-Butyl alcohol	0	–
18	Co-MCM-41	Monochlorbenzene	Trace	–

[a] Reaction conditions: catalyst, 0.2 g; reaction temperature, 373 K; styrene, 10 mmol; solvent, 20 ml; flow rate of O_2, 3.0 ml min^{-1}; reaction time, 4 h.

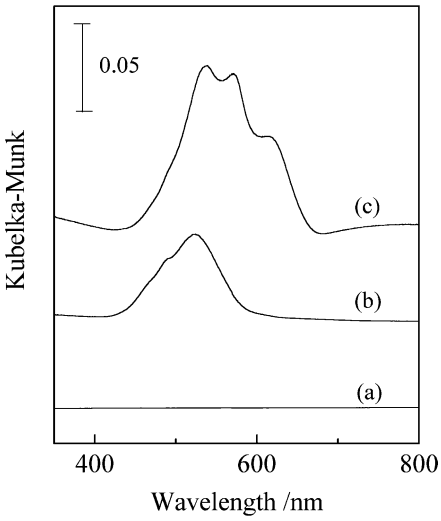

Fig. 10. Diffuse reflectance UV–vis spectra: (a) NaX, (b) Co^{2+}–NaX (Co, 8.8 wt%), (c) Co^{2+}–NaX–DMF adduct.

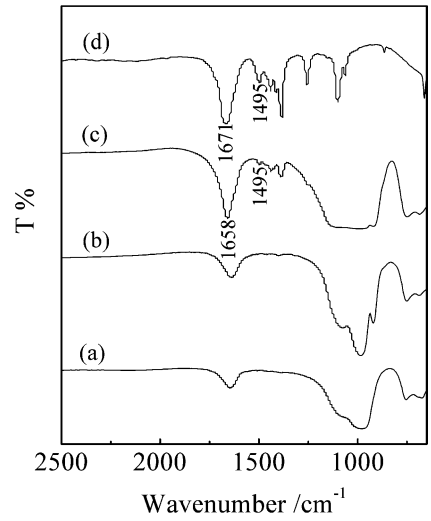

Fig. 11. FTIR spectra: (a) NaX, (b) Co^{2+}–NaX (Co, 8.8 wt%), (c) Co^{2+}–NaX–DMF adduct, (d) DMF.

In our experiment, we prepared a Co^{2+}–NaX-DMF adduct by treating the Co^{2+}–NaX (Co, 8.8 wt%, pink powder) in DMF (20 ml) at room temperature for 2 h and then at 373 K for 2 h followed by filtration, and washing thoroughly with CH_2Cl_2 to remove the excess DMF. The CH_2Cl_2 was finally removed by evacuation. The elemental analyses for the blue powder obtained revealed that the molar ratios of C/N and C/Co were 3.1 and 0.78, respectively. These results probably suggest that one DMF molecule is coordinated to one Co(II) site, and only 78% of all of the Co(II) sites have the chance to bind DMF. This is reasonable since the Co(II) sites in the small cages may not bind DMF molecules. Fig. 10 compares the DRUV–vis spectrum of the Co^{2+}–NaX-DMF adduct with those of the Co^{2+}–NaX and NaX. No band appeared for NaX in the range of 250–800 nm, whereas an absorption band at 520 nm was observed for the Co^{2+}–NaX sample. This band is typical of Co^{2+} in octahedral symmetry and can be attributed either to $[Co(H_2O)_6]^{2+}$ or to $[Co(H_2O)_5OH]^{+}$ located in the cavities of zeolites [73,74]. For the Co^{2+}–NaX-DMF adduct, three bands at 537, 571, and 615 nm were observed. It should be noted that there is no absorption band for DMF alone at 350–800 nm. Thus it is clear that the coordination environment of cobalt has been changed via DMF treatment. It is known that Co^{2+} in a tetrahedral coordination with d^7 configuration, such as Co^{2+} in CoAPO-5 and Co-APO-11, exhibits a triplet of bands at about 540, 578, and 625 nm, which are caused by Jahn–Teller distortions and/or by spin-orbit coupling during the spin-allowed $^4A_2 \rightarrow {}^4T_1$ transition [75,76]. The positions of these bands are almost the same as those observed for the Co^{2+}–NaX-DMF adduct. Therefore, the coordination of DMF to Co^{2+} in the zeolite has changed the coordination of cobalt from octahedral to tetrahedral symmetry.

Fig. 11 shows a FTIR spectrum for the Co^{2+}–NaX-DMF adduct along with those for NaX, Co^{2+}–NaX, and DMF. NaX exhibits bands at 980–1100 cm^{-1} and 670–760 cm^{-1} ascribed to the antisymmetrical and symmetrical vibration of framework T–O–T bonds (SiO_4 or AlO_4) and a band at 1630 cm^{-1} for adsorbed water [77,78]. For the Co^{2+}–NaX, an additional absorption band appeared at 921 cm^{-1}. This band can be attributed to the perturbed T–O–T antisymmetrical mode caused by Co^{2+} at the cationic sites [77–79]. On the other hand, the free DMF presents a strong band at 1671 cm^{-1} and a medium-strength band at 1495 cm^{-1}, which were attributed to the C=O stretching and the C–N stretching of O–C–N of DMF, respectively [80]. Other bands ascribed to the CH_3 deforming vibration and the stretching of N–C of C–N–C of DMF at 1440, 1382, 1260, and 1100 cm^{-1} were also observed [80]. It has been reported that the C=O stretching band of DMF is of great significance in the study of bonding and coordination of DMF, and the shift of this band to a lower frequency has been found upon coordination to several transition metal ions due to the bonding of DMF to the metals through oxygen [68]. We observed a meaningful shift of the C=O stretching vibration from 1671 cm^{-1} for the free DMF to 1658 cm^{-1} for the Co^{2+}–NaX-DMF adduct, whereas the band for C–N at 1495 cm^{-1} did not undergo significant shift. Therefore, it is probable that DMF is coordinated to the Co^{2+} located inside the supercage of the zeolite through oxygen. We may speculate that there is a similar coordination of DMF to the single-site Co(II) site located in the mesoporous channels of MCM-41.

It should be recalled here that, in homogeneous epoxidation reactions, $Co(Ac)_2$ and $Co(NO_3)_2$ were almost inactive for the conversion of styrene, whereas $CoCl_2$ exhibited some activity, although the catalytic performances were lower than those of the Co^{2+}–NaX or the Co-MCM-41 (Table 2). We have clarified that this may be related to the difference in the coordination of DMF to these cobalt salts in DMF solutions. As $CoCl_2$ was added to DMF, an obvious change

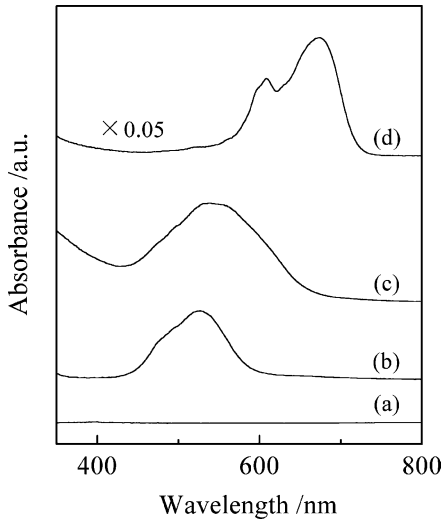

Fig. 12. UV–vis spectra: (a) DMF, (b) $Co(NO_3)_2$–DMF, (c) $Co(Ac)_2$–DMF, (d) $CoCl_2$–DMF.

in color from pink to blue was observed, whereas the pink color remained unchanged after the addition of $Co(Ac)_2$ or $Co(NO_3)_2$ to DMF. As shown in Fig. 12, the UV–vis spectrum of $CoCl_2$ in DMF solution corresponded well to Co^{2+} ions in a typical tetrahedral coordination [81]. The formation of a $CoCl_2$–DMF complex ($Co_2Cl_4 \cdot 2DMF \cdot 2H_2O$) with Co^{2+} in tetrahedral coordination was reported previously [68]. On the other hand, the Co^{2+} remained in octahedral coordination after $Co(Ac)_2$ or $Co(NO_3)_2$ was added to DMF. Therefore, it seems that the tetrahedrally coordinated Co^{2+} sites including DMF ligand play an important role in the activation of O_2 for epoxidation reactions.

3.8. Possible reaction mechanism

We have found that the epoxidation of many other unfunctionalized alkenes such as methylstyrene, stilbene, and cyclooctene with O_2 can also proceed over the Co^{2+}–NaX and the Co-MCM-41 catalysts. *trans*-Stilbene could be converted into *trans*-stilbene oxide with a high selectivity (> 90%) even at a high conversion of the substrate. However, in the epoxidation of *cis*-stilbene, *trans*-stilbene oxide was mainly formed over both catalysts. This result is different from that for the epoxidation of *cis*-stilbene with TBHP catalyzed by the Ti-MCM-41 prepared by a surface grafting method where only *cis*-stilbene oxide has been obtained, and thus it is argued that the reaction proceeds through a radical-free mechanism [82]. On the other hand, *cis*-stilbene was mainly converted to *trans*-stilbene oxide and benzaldehyde with TBHP over the Mn-MCM-41 prepared by the TIE method, indicating the possible formation of a radical intermediate during the reaction [46,83]. In the present O_2- and the cobalt-containing molecular sieve-based catalytic system, *trans*-stilbene oxide has been observed as the main product in the epoxidation of *cis*-stilbene. Furthermore, we have confirmed that the isomerization of *cis*-stilbene to *trans*-stilbene and that of *cis*-stilbene oxide to *trans*-stilbene oxide do not take place in the absence of O_2 under the reaction conditions. Thus it is reasonable to speculate that the active oxygen in the current system possesses a radical nature. The radical intermediate formed after the attack of the active oxygen may have a long enough lifetime to rotate around the single carbon–carbon bond to undergo isomerization. *trans*-Stilbene oxide has mainly been obtained because the *trans*-isomer is thermodynamically more stable than the *cis*-isomer.

To clarify this point, the influence of the addition of a radical scavenger, butyl hydroxy toluene (BHT), on catalytic performances has been investigated. The results revealed that, over both the Co^{2+}–NaX (Co, 8.8 wt%) and the Co-MCM-41 (Co, 0.78 wt%) catalysts, styrene conversion decreased to almost zero after the addition of a small amount of BHT (ca. 0.05 mmol) under the reaction conditions shown in Table 4. This observation confirms the radical nature of the active oxygen species formed by the activation of O_2 over the tetrahedral Co(II) site.

It is well known that many Co(II) complexes can bind and activate O_2 to form complexes comprising Co(III)–(O_2^-) [84]. We speculate that, in our case, a similar binding of O_2 to the Co(II) sites located in the molecular sieves may also occur in the initial step. The Co(III)–(O_2^-) species formed might undergo further reactions to generate an active oxygen species with a radical nature responsible for the epoxidation. It is known that Co(III) ions may catalyze the formation of an acylperoxy radical from benzaldehyde by O_2 [38]. The acylperoxy radical may epoxidize alkenes to give epoxides and benzoic acid. In our case, although benzaldehyde was formed as a main by-product, we did not observe the formation of a significant amount of benzoic acid. Moreover, the epoxidation was not significantly enhanced when an excess of benzaldehyde was added to the reactant mixture. Therefore, we can exclude the possibility that benzaldehyde may act as the co-reductant. However, DMF itself may act as a co-reductant in the formation of active oxygen species. This possibility still remains at this moment. Further elucidation of this point and the nature of active oxygen species is needed in future studies.

4. Conclusions

It has been clarified through detailed characterizations that cobalt introduced into MCM-41 by the template-ion exchange method exists in a coordination environment similar to that in the faujasite zeolite and exists mainly in the single-site Co(II) state on the inner surface of molecular sieves. On the other hand, the samples prepared by the impregnation method contain aggregated Co_3O_4 particles located outside the cavities of molecular sieves. The Co(II) sites located in faujasite or MCM-41 can catalyze the epoxidation of styrene by oxygen with higher efficiency than Co_3O_4 and the Co^{2+} ions in the liquid phase. Oxygen is found to be a

better oxidant for epoxidation reactions than H_2O_2, TBHP, and NaClO over Co(II)-containing molecular sieves, and the solvent (DMF) plays a crucial role in the reaction through the coordination to the Co(II) site, forming a tetrahedral DMF-coordinated Co(II) active site. An oxygen species with a radical nature produced via the activation of molecular oxygen has been proposed for the epoxidation reactions.

Acknowledgments

This work was supported by the National Basic Research Program of China (No. 2003CB615803) and the National Natural Science Foundation of China (Nos. 20021002, 20273054, and 20373055).

References

[1] J.-M. Brégeault, Dalton Trans. (2003) 3289.
[2] M.G. Clerici, G. Bellussi, U. Romano, J. Catal. 129 (1991) 159.
[3] A. Corma, H. Garcia, Chem. Rev. 102 (2002) 3837.
[4] B.S. Lane, K. Burgess, Chem. Rev. 103 (2003) 2457.
[5] I.W.C.E. Arends, R.A. Sheldon, Top. Catal. 19 (2002) 133.
[6] G. Grigoropoulou, J.H. Clark, J.A. Elings, Green Chem. 5 (2003) 1.
[7] R. Rinaldi, U. Schuchardt, J. Catal. 227 (2004) 109.
[8] R. Meiers, U. Dingerdissen, W.F. Hölderich, J. Catal. 176 (1998) 376.
[9] T.A. Nijhuis, B.J. Huizinga, M. Makkee, J.A. Moulijin, Ind. Eng. Chem. Res. 38 (1999) 884.
[10] T. Hayashi, K. Tanaka, M. Haruta, J. Catal. 178 (1998) 566.
[11] B.S. Uphade, T. Akita, T. Nakamura, M. Haruta, J. Catal. 209 (2002) 331.
[12] M.P. Kapoor, A.K. Sinha, S. Seelan, S. Inagaki, S. Tsubota, H. Yoshida, M. Haruta, Chem. Commun. (2002) 2902.
[13] A.K. Sinha, S. Seelan, S. Tsubota, M. Haruta, Angew. Chem. Int. Ed. 43 (2004) 1546.
[14] I. Yamanaka, K. Nakagaki, K. Otsuka, J. Chem. Soc. Chem. Commun. (1995) 1185.
[15] B. Meunier, Chem. Rev. 92 (1992) 1411.
[16] M.G. Clerici, P. Inagallina, Catal. Today 41 (1998) 351.
[17] T. Iwahama, G. Hatta, S. Sakaguchi, Y. Ishii, Chem. Commun. (2000) 163.
[18] Y. Liu, K. Murata, M. Inaba, Chem. Commun. (2004) 582.
[19] W.F. Hölderich, F. Lollmer, Pure Appl. Chem. 72 (2000) 1273.
[20] V. Duma, D. Hönicke, J. Catal. 191 (2000) 93.
[21] R. Ben-Daniel, L. Weiner, R. Neumann, J. Am. Chem. Soc. 124 (2002) 8788.
[22] X. Wang, Q. Zhang, Q. Guo, Y. Lou, L. Yang, Y. Wang, Chem. Commun. (2004) 1396.
[23] J.T. Groves, R. Quinn, J. Am. Chem. Soc. 107 (1985) 5790.
[24] A.S. Goldstein, R.H. Beer, R.S. Drago, J. Am. Chem. Soc. 116 (1994) 2424.
[25] R. Neumann, M. Dahan, Nature 388 (1997) 353.
[26] Y. Nishiyama, Y. Nakagawa, N. Mizuno, Angew. Chem. Int. Ed. 40 (2001) 3639.
[27] R.A. Sheldon, J.K. Kochi, Metal-Catalyzed Oxidation of Organic Compounds, Academic, New York, 1981.
[28] J.E. Lyons, ACS Adv. Chem. Ser. 132 (1974) 64.
[29] R.A. Budnik, J.K. Kochi, J. Org. Chem. 41 (1976) 1384.
[30] M.T. Reetz, K. Töllner, Tetrahedron Lett. 36 (1995) 9461.
[31] J.D. Koola, J.K. Kochi, J. Org. Chem. 52 (1987) 4545.
[32] H. Yang, S. Qin, Z. Liu, Z. Zhou, J. Li, X. Lu, Huaxue Yanjiu Yu Yingyong 10 (1998) 86.
[33] B. Rhodes, S. Rowling, P. Tidswell, S. Woodward, S.M. Brown, J. Mol. Catal. A 116 (1997) 375.
[34] J.M. Thomas, R. Raja, Chem. Commun. (2001) 675, and references therein.
[35] U. Schuchardt, D. Cardoso, R. Sercheli, R. Pereira, R.S. Cruz, M.C. Guerreiro, D. Mandelli, E.V. Spimace, E.L. Pires, Appl. Catal. A 211 (2001) 1, and references therein.
[36] I. Belkhir, A. Germain, F. Fajula, E. Fache, J. Chem. Soc., Faraday Trans. 94 (1998) 1761.
[37] A.F. Masters, J.K. Beattie, A.L. Roa, Catal. Lett. 75 (2001) 159.
[38] R. Raja, G. Sankar, J.M. Thomas, Chem. Commun. (1999) 829.
[39] T. Yamada, T. Takai, O. Rhode, T. Mukaiyama, Chem. Lett. (1991) 1.
[40] D. Dhar, Y. Koltypin, A. Gedanken, S. Chandrasekaran, Catal. Lett. 86 (2003) 197.
[41] T. Pruß, D.J. Macquarrie, J.H. Clark, Appl. Catal. A 276 (2004) 29.
[42] Q. Tang, Y. Wang, J. Liang, P. Wang, Q. Zhang, H. Wan, Chem. Commun. (2004) 440.
[43] Q. Tang, Q. Zhang, P. Wang, Y. Wang, H. Wan, Chem. Mater. 16 (2004) 1967.
[44] M. Yonemitsu, Y. Tanaka, M. Iwamoto, Chem. Mater. 9 (1997) 2679.
[45] M. Iwamoto, Y. Tanaka, Catal. Surv. Jpn. 5 (2001) 25.
[46] Q. Zhang, Y. Wang, S. Itsuki, T. Shishido, K. Takehira, J. Mol. Catal. A 188 (2002) 189.
[47] Y. Wang, Q. Zhang, Y. Ohishi, T. Shishido, K. Takehira, Catal. Lett. 72 (2001) 215.
[48] Q. Zhang, Y. Wang, Y. Ohishi, T. Shishido, K. Takehira, J. Catal. 202 (2001) 308.
[49] N. Lang, P. Delichere, A. Tuel, Micropor. Mesopor. Mater. 56 (2002) 203.
[50] A.B. Bourlinos, M.A. Karakassides, D. Petridis, J. Phys. Chem. B 104 (2000) 4375.
[51] Y. Wang, Q. Zhang, T. Shishido, K. Takehira, J. Catal. 209 (2002) 186.
[52] Y. Wang, Y. Ohishi, T. Shishido, Q. Zhang, W. Yang, Q. Guo, H. Wan, K. Takehira, J. Catal. 220 (2003) 347.
[53] G. Xiong, Z. Feng, J. Li, Q. Yang, P. Ying, Q. Xin, C. Li, J. Phys. Chem. B 104 (2000) 3581.
[54] M.A. Vuurman, D.J. Stufkens, A. Oskam, G. Deo, I.E. Wachs, J. Chem. Soc., Faraday Trans. 92 (1996) 3259.
[55] L. Guczi, D. Bazin, Appl. Catal. A 188 (1999) 163.
[56] L. Guczi, Catal. Lett. 7 (1991) 205.
[57] Z. Zhang, W.M.H. Sachtler, S.L. Suib, Catal. Lett. 2 (1989) 395.
[58] V. Schwartz, R. Prins, X. Wang, W.M.H. Sachtler, J. Phys. Chem. B 106 (2002) 7210.
[59] P. Arnoldy, J.A. Moulijin, J. Catal. 93 (1985) 38.
[60] L.A. Boot, M.H.J.V. Kerkhoffs, A.J. van Dillen, J.W. Geus, F.R. van Buren, B.T. van der Linden, Appl. Catal. A 137 (1996) 69.
[61] S. Sun, N. Tsubaki, K. Fujimoto, Appl. Catal. A 202 (2000) 121.
[62] S. Buttefey, A. Boutin, C. Mellot-Draznieks, A.H. Fuchs, J. Phys. Chem. B 105 (2001) 9569.
[63] S.H. Lee, Y. Kim, K. Seff, J. Phys. Chem. B 104 (2000) 2490.
[64] D. Bae, K. Seff, Micropor. Mesopor. Mater. 33 (1999) 265.
[65] H. Praliaud, G. Coudurier, J. Chem. Soc., Faraday Trans. I 75 (1979) 2601.
[66] R.A. Sheldon, M. Wallau, I.W.C.E. Arends, U. Schuchardt, Acc. Chem. Res. 31 (1998) 485, and references therein.
[67] Y.H. Lin, I.D. Williams, P. Li, Appl. Catal. A 150 (1997) 221.
[68] V.T. Yilmaz, Y. Topcu, Thermochim. Acta 307 (1997) 143.
[69] M. Koide, S. Ishiguro, Z. Naturfors. Sect. A, J. Phys. Sci. 50 (1995) 11.
[70] H. Yokoyama, S. Suzuki, M. Goto, K. Shinozaki, Y. Abe, S. Ishiguro, Z. Naturfors. Sect. A, J. Phys. Sci. 50 (1995) 301.
[71] E. Eichhorn, A. Rieker, B. Speiser, H. Stahl, Inorg. Chem. 36 (1997) 3307.
[72] A. Pui, Croat. Chem. Acta 75 (2002) 165.
[73] G. Fierro, M.A. Eberhardt, M. Houalla, D.M. Hercules, W.K. Hall, J. Phys. Chem. 100 (1996) 8468.
[74] El-M. Elmalki, D. Werst, P.E. Doan, W.M.H. Sachtler, J. Phys. Chem. 104 (2000) 5924.

[75] A.A. Verberckmoes, B.M. Weckhuysen, R.A. Schoonheydt, Micropor. Mesopor. Mater. 22 (1998) 165.
[76] J. Šponer, J. Čejka, J. Dědeček, B. Wichterlová, Micropor. Mesopor. Mater. 37 (2000) 117.
[77] Z. Sobalík, Z. Tvarůžková, B. Wichterlová, J. Phys. Chem. B 102 (1998) 1077.
[78] L. Drozdová, R. Prins, J. Dědeček, Z. Sobalík, B. Wichterlová, J. Phys. Chem. B 116 (2002) 2240.
[79] J. Dědeček, L. Čapek, D. Kaucký, Z. Sobalík, B. Wichterlová, J. Catal. 211 (2002) 198.
[80] E.W. Randall, C.M.S. Yoder, J.J. Zuckerman, Inorg. Chem. 5 (1966) 2240.
[81] F.A. Cotton, G. Wilkinson, in: Advanced Inorganic Chemistry, Willey, New York, 1972, p. 881.
[82] R.D. Oldroyd, J.M. Thomas, T. Maschmeyer, P.A. MacFaul, D.W. Snelgrove, K.U. Ingold, D.D.W. Wayner, Angew. Chem. Int. Ed. Eng. 35 (1996) 2787.
[83] M. Yonemitsu, Y. Tanaka, M. Iwamoto, J. Catal. 178 (1998) 207.
[84] R.D. Jones, D.A. Summerville, F. Basolo, Chem. Rev. 79 (1979) 139.